Collective rotational tunneling of methyl groups and quantum solitons in 4-methylpyridine: Neutron scattering studies of single crystals

François Fillaux* and Béatrice Nicolaï
LADIR-CNRS, UMR 7075, Université Pierre et Marie Curie, 2 rue Henry Dunant, 94320 Thiais, France

Werner Paulus
LCSIM, UMR 6511, Université de Rennes I, Campus de Beaulieu, Avenue du Général Leclerc, 35042 Rennes cedex, France

Erika Kaiser-Morris and Alain Cousson
Laboratoire Léon Brillouin, CEA-CNRS, CE Saclay, 91191 Gif-sur-Yvette cedex, France
(Received 12 June 2003; published 9 December 2003)

The structure of the 4-methylpyridine crystal has been determined at 10 and 260 K with the single-crystal neutron-diffraction technique. The space-group symmetries are $I4_1/a$ and $I4_1/amd$, respectively. In both cases, there are eight molecular entities in the unit cell. The rotational axes of the methyl groups are aligned along the *c* axis. The shortest intermolecular distances occur between face-to-face methyl groups. The next shortest distances correspond to infinite chains of rotors parallel to the orthogonal axes *a* and *b*. The angular probability densities of the methyl groups are clear evidence of orientational disorder. The incoherent scattering function $S(Q_a, Q_b, \omega)$ has been measured with the inelastic neutron scattering technique at 1.7 K. The energy-transfer ranges, $\hbar\omega = \pm(500 \pm 60)\mu$eV, encompass transitions due to rotational tunneling. The anisotropy in **Q** is distinctive of dynamics in one dimension. These are represented with the quantum sine-Gordon equation that is an approximation to the Hamiltonian for an infinite chain of coupled rotors. Spots of intensity observed for neutron-energy loss at $|Q_a|$ or $|Q_b| \approx 1.55$ Å^{-1} are distinctive of stationary states for breathers. Weaker peaks at $|Q_a|$ or $|Q_b| \approx 1.0$ Å^{-1} reveal collective tunneling. This is a thermally activated process arising from rather heavy pseudoparticles composed of large numbers (from 22 to 25) of kinks or antikinks. Quantization of the kinetic momentum arises from the chain discreteness and from conservation of the angular momentum. Traveling states are stationary when the kinetic energy is within the tunneling energy band. In the ground state, the chain dynamics are represented with a single collective angular coordinate. The incoherent scattering function for neutron-energy-gain reveals bound excited states with lifetimes of several days.

DOI: 10.1103/PhysRevB.68.224301 PACS number(s): 63.20.Dj, 25.40.Dn, 33.20.Tp

I. INTRODUCTION

Nonlinear excitations giving rise to spatially localized nondissipative waves in an extended lattice could be a source of phenomena and technological principles in advanced materials research.[1–3] They are also speculated key elements in complex events on the molecular level of life functioning.[4,5] Vibrational spectroscopy techniques have great potential for observing nonlinear excitations of atoms and molecules. However, most of the spectra are convincingly rationalized within the framework of the (quasi)harmonic approximation (namely, normal modes and phonons). Only spectra of highly anharmonic degrees of freedom (for example, proton motions in hydrogen bonds, rotational tunneling, etc.) deserve tentative approaches in terms of nonlinear excitations but, even for these pathological cases, there is no well-established fingerprint distinctive of nonlinear dynamics. The spectroscopic signature of quantum analogs to classical ''spatially localized nondissipative waves'' is barely known, and still a matter of controversy because, in many cases, the confrontation of theoretical models with experiments is hampered by the complexity of the environment in solids.

The spectroscopic studies of nonlinear dynamics in a molecular crystal reported below highlight the correspondence between classical nonlinear excitations and eigenstates for quantum pseudoparticles. The confrontation of theory and experiments benefits from the remarkable suitability of the dynamical model (the sine-Gordon equation) to the crystal structure and dynamics (collective rotational tunneling of methyl groups in one dimension), and from the great specificity of the inelastic neutron scattering (INS) technique. These advantages are further documented below.

The *sine-Gordon equation*, among nonlinear models, covers a vast area of applications such as relativistic quantum field theory, dislocations in solids, Josephson junction arrays, charge-density waves, liquid crystals, methyl rotation, etc. In the continuous limit of the classical regime, spatially localized nonlinear nondissipative waves such as kinks, antikinks, and breathers are analytical solutions of this integrable system.[6,7] The stability and dynamics of these solitons are well documented. Moreover, exact semiclassical (WKB) quantization sheds light onto the quantum regime:[8] classical solitons become dimensionless pseudoparticles; energies at rest are renormalized; and the continuum of mass states of the classical breather gives a discrete spectrum.

The *4-methylpyridine crystal* (4MP or γ-picoline, C_6H_7N) is an ideal system for experimental studies of nonlinear dynamics arising from collective rotation of methyl groups.[9–12] For the isolated molecule (Fig. 1) the methyl group bound to the pyridine ring rotates almost freely around

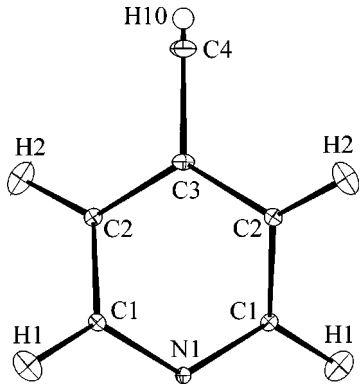

FIG. 1. Schematic view of the 4-methylpyridine molecule, showing anisotropic temperature factors and atom numbering. The three protons of the C4 methyl group are fully disordered. They are referred to as H10 in the crystal structure analysis (see below Sec. II).

the C—C single bond. In the crystalline state these rotors are organized in infinite chains with rotational axes parallel to the *c* crystal axis (see Fig. 2 and below, Sec. II).[13–15] The crystal symmetry discards coupling between equivalent chains parallel to either *a* or *b* axis. To the best of our knowledge, this structure is unique to observing collective quantum rotation in one dimension. These dynamics can be confronted with the quantum sine-Gordon equation applied to infinite chains of threefold rotors with quadratic coupling between nearest neighbors.

Tunneling spectroscopy is distinctive of quantum rotational dynamics of methyl groups.

(i) In the frequency range of rotational tunneling ($\approx \pm 500$ μeV for 4MP) there is no phonon, other than the acoustic ones, arising from the crystal lattice. Consequently, interaction of rotational and lattice dynamics can be largely ignored.

(ii) The specificity of tunneling transitions to methyl rotation can be fully exploited with INS because the incoherent cross section is much greater for the hydrogen atom than for any other atom. The singling out of H atoms, further enhanced by the very large angular amplitude associated with methyl tunneling, makes the assignment of spectra quite easy.

(iii) Regarding the comparatively modest cross section of the deuterium (^{2}H) atom, partial deuteration and isotope mixtures provide information on methyl rotation. Needless to say, the many advantages of INS are complementary to those of infrared and Raman spectroscopy.[16,17]

The main INS bands observed at $\approx \pm 500$ μeV for the 4-methylpyridine crystal have been consistently interpreted in terms of quantum sine-Gordon breathers regarded as dimensionless pseudoparticles moving along single chains. The assignment scheme was based on INS spectra of isotope mixtures,[9,12] partially deuterated analogs,[10] high resolution in energy,[11] and infrared and Raman spectra.[16] It was thus emphasized that the quantum analog to a spatially localized soliton moving along a discrete chain is a stationary planar wave. As anticipated from basic principles of quantum mechanics, classical localization does not survive for pseudoparticles in the quantum regime.

Furthermore, the sine-Gordon equation is only an approximation to the real Hamiltonian and rotational dynamics in the crystal are more complex. Owing to proton indistinguishability, the chains are invariant with respect to the rotation of any top by $\pm 2\pi/3$, and the quadratic coupling in the sine-Gordon equation is only an approximation to the true periodicity of the coupling potential.[18] The topological degeneracy gives rise to collective tunneling that is not included in the sine-Gordon equation. This was tentatively represented with extended states in a continuous energy-band structure,[9] but this is actually in conflict with the slow decay of intensity observed for the supposedly tunneling bands.[11] Therefore, the question at the heart of this work is: ''What is the relevant representation of collective tunneling in an infinite chain of coupled quantum rotors?''

Previous INS studies were carried out on powdered samples. The measured scattering function $S(\mathbf{Q},\omega)$ was averaged over all crystal orientations with respect to the neutron momentum-transfer vector $\mathbf{Q}$. (By definition, $\mathbf{Q}=\mathbf{k}_0-\mathbf{k}_f$, with wave vectors $|\mathbf{k}_0|=2\pi/\lambda_0$ and $|\mathbf{k}_f|=2\pi/\lambda_f$, where λ_0 and λ_f are the incident and scattered wavelengths, respectively.) Therefore, the dispersion in $\mathbf{Q}$, an important information for quantum pseudoparticles, was unknown. However, $S(\mathbf{Q},\omega)$ for breathers traveling along chains parallel to *a* or *b* axis should show marked anisotropy: the inten-

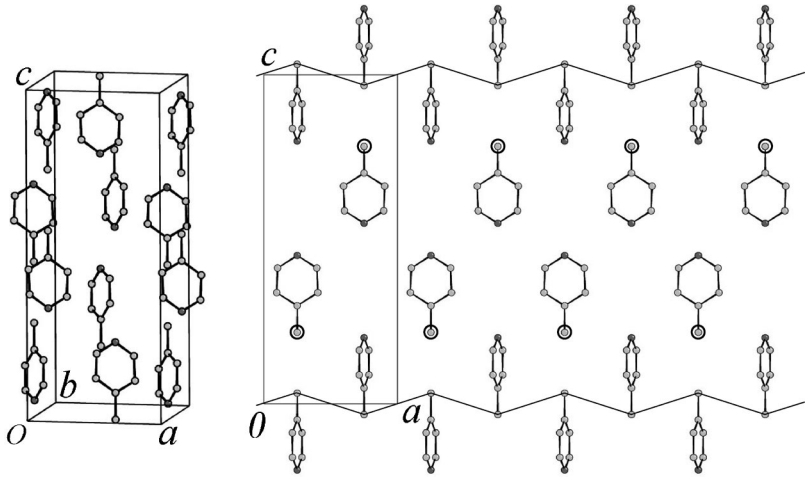

FIG. 2. Schematic view of the structure of the 4-methylpyridine crystal at 10 K. Left: the unit cell. Right: projection onto the (a,c) plane showing the infinite chains parallel to *a* (along the zigzag line) or parallel to *b* (circles). For the sake of clarity H atoms are hidden.

TABLE I. Neutron single-crystal diffraction data and structure refinement for 4-methylpyridine at 10 and 260 K. $\lambda = 0.8305$ Å. The variance for the last digit is given in parentheses.

	10 K	260 K
Space group	$I4_1/a$	$I4_1/amd$
a(Å)	7.552(8)	7.739(4)
c(Å)	18.556(1)	18.766(5)
Volume (Å^3)	1058.3(16)	1123.9(9)
Z	8	8
Reflections measured	2208	1151
Independent reflections	1721	307
Reflections used	1195	123
$\sigma(I)$ limit	3.00	3.00
Refinement on F		
R factor	0.0403	0.0403
Weighted R factor	0.0412	0.0230
Number of parameters	57	41
Goodness of fit	1.1227	1.0468

sity should be a maximum for momentum transfer parallel to the chain directions. In contrast to this, the scattering function for uncoupled methyl groups or for stationary rotating modes (also referred to as rotobreathers, Ref. 18) should be isotropic in the rotational plane (see below, Sec. III). Therefore, we have measured $S(\mathbf{Q},\omega)$ on properly oriented single crystals, such that $\mathbf{Q}$ was parallel to the (a,b) rotational plane. As a prerequisite we have also determined the structure and the angular distribution of the methyl protons at 10 K and 260 K, with the single-crystal neutron-diffraction technique.

The organization of the paper is the following. The crystal structure determination is presented in Sec. II. Then, presentation of the theoretical model (Sec. III) and of INS measurements (Sec. IV) introduce the measured maps of intensity presented in Sec. V for both neutron-energy loss (Stokes) and neutron-energy gain (anti-Stokes). The marked anisotropy of the scattering function emphasizes the one-dimensional character of the quantum dynamics. The existence of extended tunneling states must be discarded. In Sec. VI we define multisolitons to account for collective rotational tunneling. We discuss the physics of collective rotation and creation/annihilation mechanisms in Sec. VII. In conclusion, we emphasize the correspondence between classical and quantum nonlinear excitations.

II. CRYSTAL STRUCTURE: EXPERIMENTS AND RESULTS

Single crystals were grown from the melt (melting point 276.8 K) by the Bridgman method. Approximately cubic samples ($\approx 3\times3\times3$ mm^3) were cut from large crystals. Each sample was loaded into an aluminum container and then mounted in a cryostat to be cooled down slowly with a flow of helium vapor. Neutron-diffraction measurements (see Table I) were carried out on a Stoe four-circle diffractometer: namely, 5C2 at the Orphée reactor (Laboratoire Léon-Brillouin, Saclay, France).[19] The structure was analyzed with the program CRYSTALS[20] utilizing scattering factors from Ref. 21. No absorption correction was made. Extinction is very small in the high-temperature phase. At low temperature, twinning precludes any refinement of extinction coefficients.

TABLE II. Atomic positions, isotropic temperature factors, and site occupancies for the 4-methylpyridine crystal at 10 K (first lines) and 260 K (second lines). The variance for the last digit is given in parentheses.

Atom	x/a	y/b	z/c	U(iso) (Å^2)	Occupancy
N(1)	0.5000	0.2500	0.20109(3)	0.0069	1.0000
	0.0000	0.2500	0.6983(2)	0.0908	1.0000
C(1)	0.3531(1)	0.2143(1)	0.16307(4)	0.0066	1.0000
	−0.1428(14)	0.2500	0.6602(4)	0.1067	1.0000
C(2)	0.3462(1)	0.2138(1)	0.08796(4)	0.0067	1.0000
	−0.149(1)	0.2500	0.5861(4)	0.0838	1.0000
C(3)	0.5000	0.2500	0.04843(4)	0.0061	1.0000
	0.0000	0.2500	0.5480(3)	0.0629	1.0000
C(4)	0.5000	0.2500	−0.03256(5)	0.0101	1.0000
	0.0000	0.2500	0.4687(3)	0.0909	1.0000
H(1)	0.2341(3)	0.1856(4)	0.19437(12)	0.0227	1.0000
	−0.263(2)	0.2500	0.6910(11)	0.1604	1.0000
H(2)	0.2219(3)	0.1857(4)	0.06016(12)	0.0228	1.0000
	−0.276(3)	0.2500	0.557(1)	0.1873	1.0000
H(10)	0.5000	0.2500	−0.05403(14)	0.0194(5)	3.0000
	0.0000	0.2500	0.4470(5)	0.090(4)	3.0000

At 10 K, the crystal symmetry is tetragonal ($I4_1/a$, $Z=8$, see Fig. 2 and Tables I–IV).[13–15] All molecules are

TABLE III. Interatomic distances in Å units and angles in degrees in 4-methylpyridine at 10 K (first lines) and 260 K (second lines). The variance for the last digit is given in parentheses.

N(1)-C(1)	1.3421(13)	N(1)-C(1)-H(1)	116.14(15)
	1.32(1)		115.3(11)
C(1)-C(2)	1.3947(9)	C(2)-C(1)-H(1)	120.02(15)
	1.391(7)		119.8(14)
C(1)-H(1)	1.091(2)	C(1)-C(2)-C(3)	119.45(8)
	1.10(2)		119.7(10)
C(2)-C(3)	1.4009(14)!	C(1)-C(2)-H(2)	120.32(15)
	1.358(8)!		120.7(12)
C(2)-H(2)	1.092(2)	C(3)-C(2)-H(2)	120.23(15)
	1.12(3)		119.6(10)
C(3)-C(4)	1.5029(12)	C(2)-C(3)-C(2)	116.9(1)
	1.489(9)		116.5(9)
C(4)-H(10)	0.398(3)	C(2)-C(3)-C(4)	121.57(7)
	0.407(12)		121.7(4)
C(1)-N(1)-C(1)	116.6(1)	C(3)-C(4)-H(10)	180.00
	114.1(10)		180.00
N(1)-C(1)-C(2)	123.84(9)		
	125.0(11)		

TABLE IV. Thermal parameters in $Å^2$ units for 4-methylpyridine at 10 K (first lines) and 260 K (second lines). The variance for the last digit is given in parentheses.

Atom	U_{11}	U_{22}	U_{33}	U_{23}	U_{13}	U_{12}
N(1)	0.0056(7)	0.0102(8)	0.00483(18)	0.0000	0.0000	−0.0036(4)
	0.082(7)	0.147(9)	0.044(2)	0.0000	0.0000	0.0000
C(1)	0.0055(2)	0.0087(2)	0.0055(2)	−0.00022(18)	0.00069(17)	−0.00040(19)
	0.107(9)	0.155(8)	0.058(4)	0.0000	0.017(4)	0.0000
C(2)	0.0060(2)	0.0085(2)	0.0056(2)	−0.00016(18)	−0.00028(18)	−0.00041(19)
	0.061(5)	0.129(7)	0.062(3)	0.0000	0.001(3)	0.0000
C(3)	0.008(1)	0.0060(9)	0.0045(3)	0.0000	0.0000	0.0034(5)
	0.095(8)	0.037(5)	0.056(3)	0.0000	0.0000	0.0000
C(4)	0.0128(4)	0.0122(4)	0.0053(3)	0.0000	0.0000	−0.0007(4)
	0.12(1)	0.104(9)	0.047(3)	0.0000	0.0000	0.0000
H(1)	0.0162(7)	0.0356(11)	0.0164(8)	0.0002(7)	0.0051(5)	−0.0050(7)
	0.07(1)	0.31(3)	0.100(11)	0.0000	0.03(1)	0.0000
H(2)	0.0141(6)	0.0352(11)	0.0191(8)	−0.0020(7)	−0.0060(6)	−0.0052(6)
	0.107(17)	0.35(4)	0.107(14)	0.0000	−0.023(12)	0.0000

equivalent and molecular planes are tilted by 13.2° with respect to the (100) and (010) planes, respectively (Fig. 3). The shortest intermolecular distances of 3.430(2) Å occur between face-to-face methyl groups. According to Ohms and co-workers,[13] paired methyl groups should be twisted by $\pm 60°$ with respect to each other and perform combined rotation. However, this is not consistent with the C_2 site symmetry. To any particular orientation of one group corresponds four indistinguishable orientations obtained by symmetry with respect to the molecular plane and by $\pm \pi/2$ rotation. The 12 equivalent proton sites are indistinguishable in the probability density obtained with the Fourier difference method (see Fig. 3, top and middle). The ideal isotropic distribution anticipated for disordered rotors with fixed axes is only slightly modified by convolution with the probability density arising from molecular librations.[22,23] Consequently, the methyl protons were represented with an isotropic ring, with total cross section equivalent to three protons, for the refinement of atomic positions. The radius of the ring and the isotropic thermal factor $U(\mathrm{iso})$ were refined independently (see Table V). We conclude that the effective intrapair potential arising from the H···H pair potential averaged over all orientations is virtually a constant. As the next shortest methyl-methyl distances of 3.956(1) Å occur parallel to *a* and *b* axes, one can distinguish two equivalent sets of orthogonal infinite chains of methyl groups. The zigzag lines in Fig. 2 correspond to chains parallel to one of the crystal axes (say a) and circles represent intersections with the (a,c) plane of chains parallel to the other axis (say b). There is only one close-contact pair in common for two orthogonal chains and coupling between collective excitations along *a* or *b* can be ignored. Rotational dynamics are largely one-dimensional in nature.[9–12]

At higher temperatures, the structure remains unchanged until the second-order phase transition at 254 K.[16,24] Above the transition, at 260 K, the symmetry is $I4_1/amd(Z=8)$ and the number of independent reflections decreases dramatically (see Table I). The main change is the rotation of the molecular planes to be parallel to the (001) and (010) planes (compare Figs. 4 and 3). Otherwise, interatomic distances, bond angles, and the chain arrangement are very little affected (see Tables II–V). The probability density for methyl-group orientations remains largely isotropic. Compared to the structure at 10 K, the weak submaxima due to convolution with molecular libration have rotated along with the molecular planes. Finally, the transition between collective and uncorrelated rotational dynamics previously observed at ≈ 100 K with Raman[16] has no visible counterpart in the diffraction pattern.

III. THEORETICAL DYNAMICAL MODEL

The Hamiltonian for an isolated infinite chain, with lattice parameter L, of coupled methyl rotors can be written as

$$H=\sum_j -\frac{\hbar^2}{2I_r}\frac{\partial^2}{\partial\theta_j^2}+\frac{V_0}{2}(1-\cos 3\theta_j) + \frac{V_c}{2}[1-\cos 3(\theta_{j+1}-\theta_j)], \quad (1)$$

where θ_j is the angular coordinate of the jth rotor. V_0 is the on-site potential and V_c is the coupling between nearest neighbors. I_r is the reduced moment of inertia.

A. Tunneling

In previous works,[9,10,12] rotational tunneling was regarded as a one-dimensional band-structure problem. Eigenstates are planar waves with longitudinal wave vector $k_\parallel$. Apart from a phase factor, wave functions can be represented with the basis set for free rotors as

$$\varphi_{0A}(k_\parallel,\theta)=(2\pi)^{-1/2}a_{0A0}(k_\parallel) + \pi^{-1/2}\sum_{n=1}^{\infty} a_{0A3n}(k_\parallel)\cos(3n\theta),$$

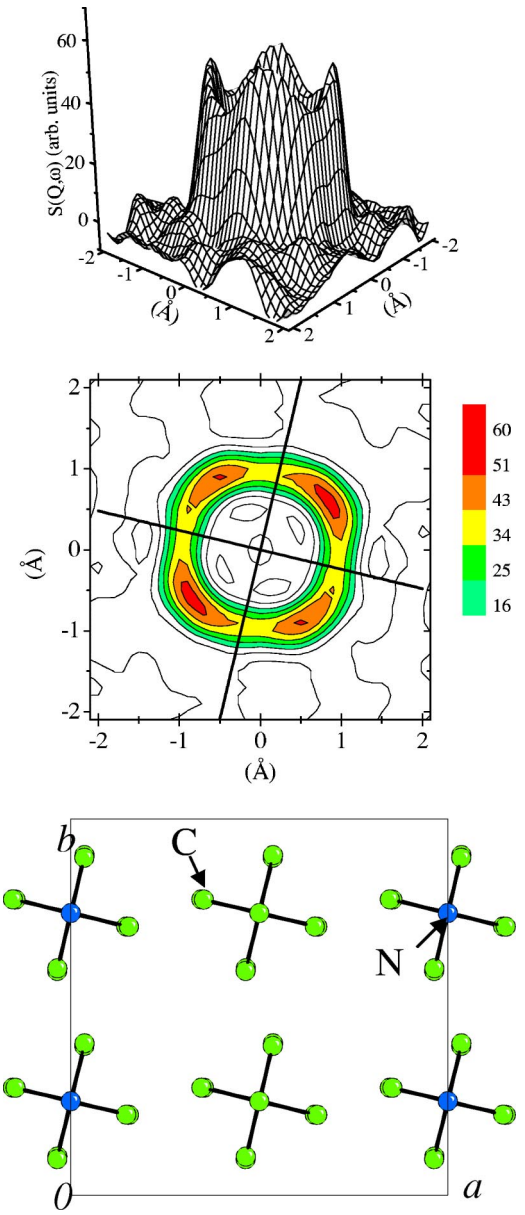

FIG. 3. (Color online) 4-methylpyridine crystal at 10 K. Bottom: projection of the crystal structure on the (a,b) plane. For the sake of clarity, H atoms are not represented. Landscape view (top) and map of isodensity contours (middle) of the H-atom distribution in the rotational plane of the methyl groups, obtained with the Fourier difference method. The solid lines represent the orientations of the molecular planes.

TABLE V. Refinement of the radius ρ, of the isotropic thermal factor $[U(\mathrm{iso})]$, and of the position of the center of the methyl proton-ring for 4-methylpyridine at 10 K (first lines) and 260 K (second lines). The variance for the last digit is given in parentheses.

Atom	ρ(Å)	$U(\mathrm{iso})$(Å)^2
H(10)	1.024(3)	0.0194(5)
	1.018(14)	0.090(4)

$$\varphi_{0E+}(k_\parallel,\theta)=\pi^{-1/2}\sum_{n=0}^{\infty}[a_{0E+(3n+1)}(k_\parallel)\cos(3n+1)\theta + a_{0E+(3n+2)}(k_\parallel)\cos(3n+2)\theta],$$

$$\varphi_{0E-}(k_\parallel,\theta)=\pi^{-1/2}\sum_{n=0}^{\infty}[a_{0E-(3n+1)}(k_\parallel)\sin(3n+1)\theta + a_{0E-(3n+2)}(k_\parallel)\sin(3n+2)\theta]. \quad (2)$$

The lowest state is $|0_A\rangle$. The degenerate tunneling states with opposite angular momentums are $|0_{E+}\rangle$ (symmetrical) and $|0_{E-}\rangle$ (antisymmetrical). The tunnel splitting, $E_{0E\pm}(k_\parallel)-E_{0A}(k_\parallel)$, varies continuously between two extremes: E_{ip}, for in-phase tunneling ($k_\parallel=0$), and E_{op}, for out-of-phase tunneling ($k_\parallel L=\pi/3$, that is, $k_\parallel\approx 0.26$Å^{-1} in the case of 4MP). The corresponding Hamiltonians are

$$H_{ip}=-\frac{\hbar^2}{2I_r}\frac{\partial^2}{\partial\theta_j^2}+\frac{V_0}{2}(1-\cos 3\theta),$$

$$H_{op}=-\frac{\hbar^2}{2I_r}\frac{\partial^2}{\partial\theta_j^2}+\frac{V_0}{2}(1-\cos 3\theta)+\frac{V_c}{2}(1-\cos 6\theta). \quad (3)$$

As these extremes correspond to the maxima of the density of states, INS transitions observed at (539 ± 4) and (472 ± 4) μeV were attributed to E_{ip} and E_{op}, respectively. Then, $V_0=3.66$ meV and $V_c=5.46$ meV.

In momentum space, the Fourier transform of the wave functions is composed of circles at $|\mathbf{k}|=(3n+1)/r$ and $(3n+2)/r$. For free rotors, there is only one circle with a radius of $|\mathbf{k}|=1/r\approx 1$ Å^{-1}. Amplitudes of high-order rings are increasing functions of the potential barrier. For the rather weak V_0 and V_c values in 4MP, numerical estimation gives more than 80% of the total amplitude in the first-order ring. The second-order ring, on the edge of the measured range, and higher orders, can be ignored. The dispersion curve at first order shows periodic oscillations between E_{ip} and E_{op} on the cylinder with radius $|\mathbf{k}|=1/r$ (see Fig. 5).

The inelastic-scattering function depends on the component of the momentum-transfer vector perpendicular to the axis of rotation, $\mathbf{Q}_r$. The intensity depends also on the component along the chain, $Q_\parallel$, via $k_\parallel$ in Eq. (2). However, measurements under consideration in this work (see below Sec. IV) were performed with limited resolution in both energy, namely, of the order of the bandwidth, and momentum, of the order of the Brillouin-zone extension. Therefore, the scattering function can be averaged over the density of states as

$$\overline{S}_{0A0E\pm}(Q_r,\omega)\simeq|\langle\overline{\varphi}_{0E\pm}(\theta)|\exp(iQ_r r\theta)|\overline{\varphi}_{0A}(\theta)\rangle|^2 \times\delta(\overline{E}_{0E\pm}-\overline{E}_{0A}-\hbar\omega). \quad (4)$$

This is nonzero if $Q_r r=n_r$ and we anticipate rings of intensity located at $Q_r\approx 1,2,\ldots$ Å^{-1}. The intensity should be located essentially at $Q_r\approx 1$ Å^{-1}.

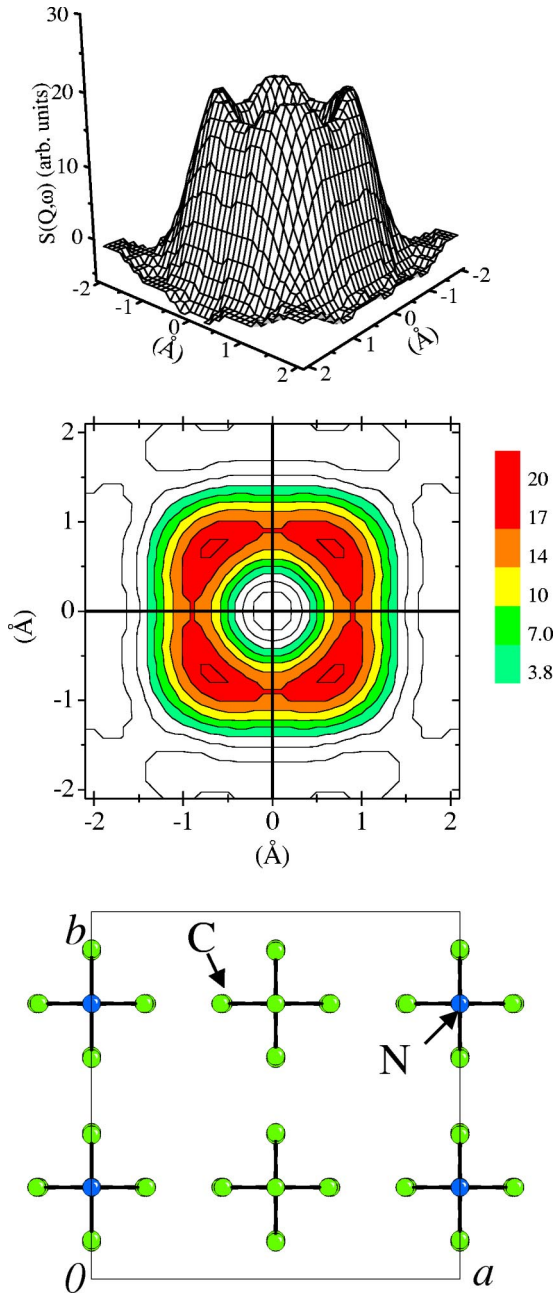

FIG. 4. (Color online) 4-methylpyridine crystal at 260 K. Bottom: projection of the crystal structure on the (a,b) plane. For the sake of clarity, H atoms are not represented. Landscape view (top) and map of isodensity contours (middle) of the H-atom distribution in the rotational plane of the methyl groups, obtained with the Fourier difference method. The solid lines represent the orientations of the molecular planes.

B. The quantum sine-Gordon breather

In the strong-coupling (or displacive) limit, $\theta_{j+1}-\theta_j$ is small, Eq. (1) can be approximated with the sine-Gordon equation

$$H \approx \sum_j -\frac{\hbar^2}{2I_r}\frac{\partial^2}{\partial\theta_j^2} + \frac{V_0}{2}(1-\cos 3\theta_j) + \frac{9V_c}{4}(\theta_{j+1}-\theta_j)^2. \tag{5}$$

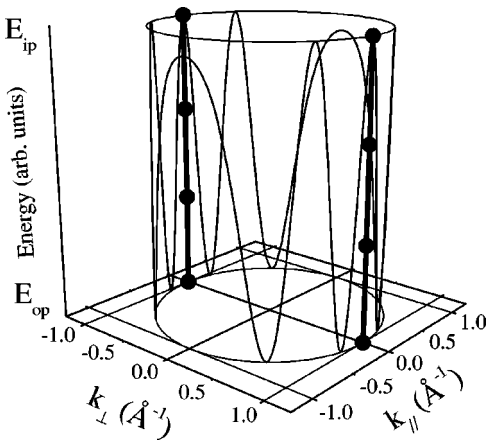

FIG. 5. Schematic representation of the dispersion of tunneling frequencies in momentum space. $k_\parallel$ and $k_\perp$ are components of the wave vectors parallel and perpendicular to the chain direction, respectively. The extension of the Brillouin zone is ± 0.26 Å^{-1}. The continuous line showing oscillations corresponds to the dispersion of Bloch's states. The vertical bold lines at $k_\perp = \pm 1$ are singularities arising from conservation of the angular momentum (see Sec. VI). Solid circles correspond to traveling states of *N*-ksolitons (see Sec. VI A).

In the continuous limit, kinks, antikinks, and breathers are exact solutions. These solitons do not interact with rotons (equivalent to phonons), which are harmonic oscillations of the chain about the equilibrium configuration. A kink or an antikink traveling along a chain rotates the methyl groups by $\pm 2\pi/3$. This is analogous to the propagation of classical jumps over the on-site potential barriers. The breather can be regarded as a bound pair in which a kink and an antikink oscillate harmonically with respect to the center of mass. All possible amplitudes of oscillation give a continuum of internal energy, below the dissociation threshold of the bound pair.

In the quantum regime,[8] the renormalized energy at rest for kinks and antikinks remains finite, $E_{0K}=4\sqrt{V_0 V_c}(1-9/8\pi)\approx 11.5$ meV, and the population density vanishes at low temperatures. On the other hand, the quantized internal oscillation of the breather gives a discrete spectrum of renormalized energies at rest. In the particular case where the on-site potential has threefold periodicity, there is only one internal state:

$$E_{0B}=2E_{0K}\sin\left[\frac{9}{16(1-9/8\pi)}\right]. \tag{6}$$

As the breather at rest belongs to the ground state of the chain, the translational degree of freedom can be excited, via momentum transfer along the chain, even at a very low temperature. Numerical calculations validate the continuous approximation for 4MP: the width of the breather wave form is much larger than L and, therefore, there is no pinning potential arising from the chain discreteness. Breathers can move along the chain like free pseudoparticles with kinetic momentum $p_B=h/\lambda_B$, where λ_B is the de Broglie wavelength. The planar wave is diffracted by the chain lattice and station-

ary states occur for the Bragg's condition: $\lambda_B = L/n_B$, $p_B = n_B h/L$, with $n_B = 0, \pm 1, \pm 2, \ldots$. The energy spectrum is then[9]

$$E_B(n_B) = \sqrt{E_{0B}^2 + n_B^2 \hbar^2 \omega_c^2}. \quad (7)$$

The INS band at 517 μeV compares favorably to the $|0\rangle \rightarrow |1\rangle$ transition estimated with $E_{0B} = 16.25$ meV and $\hbar\omega_c = 4.13$ meV.[12] The quantized sine-Gordon breather gives a very good approximation to solutions, presumably solitonlike, of the fully periodic Hamiltonian (1). The scattering function for this transition should be a Dirac-like function for momentum transfer parallel to the chain directions and such that Q_a or $Q_b = 2\pi/L \approx 1.57$ Å^{-1}.

IV. INS SPECTRA: EXPERIMENTS

The neutron scattering experiments were carried out on the IN5 time-of-flight spectrometer at the Institut Laue-Langevin (Grenoble, France).[25] The chosen incident wavelength of 4.9 Å (incident energy $E_i = 3.37$ meV) is a compromise with the best incident neutron flux, the energy resolution (≈ 120 μeV for elastic scattering), and the accessible $|\mathbf{Q}|$ range up to ≈ 2 Å^{-1}.

The c axis of an approximately cubic single crystal ($\approx 3 \times 3 \times 3$ mm^3) was oriented perpendicular to the equatorial midplane of the detector bank containing the incident beam. The sample mounted in a cylindrical aluminum can of 10 mm diameter was loaded into a liquid-helium cryostat. The temperature was controlled at (1.7 ± 0.2) K. Measurements were carried out for various orientations of the incident wave vector $\mathbf{k}_0$ by rotating the crystal by steps of $\pm(22.5 \pm 3)°$ (see Fig. 6). The counting time was ≈ 12 h for each run and measurements of a half plane were completed within four days.

Using standard values, the incoherent-scattering cross section per volume unit is ≈ 4.1 cm^{-1}. About 70% of the incident neutrons undergo at least one scattering event and $\approx 45\%$ of these neutrons undergo multiple scattering. In order to estimate the contribution of multiple scattering to the spectra, let ρ and $1-\rho$ be the probabilities for inelastic- and elastic-scattering events, respectively. Inelastic scattering occurs only for momentum transfer parallel to the equatorial plane where the detector coverage (from ≈ 0 to 135°) is ≈ 0.375. The probability to detect a single inelastic-scattering event is $\approx 0.55 \times 0.375\rho \approx 0.21\rho$. Elastic scattering is virtually isotropic and the aperture of the detector bank perpendicular to the equatorial plane is not greater than $\pm 15°$. Less than 8% of neutrons undergoing successive elastic-inelastic scattering may reach the detectors with probability of 0.375. The probability of detecting such multiple-scattering events is $\approx 0.45 \times 0.08 \times 0.375\rho(1-\rho) < 0.013\rho$. The probability for higher-order processes is negligible. Therefore, multiple-scattering events give a flat background amounting to less than 2% of the total useful signal.

The $S(Q_a, Q_b, \omega)$ maps of intensity (see below) were obtained by standard conversion from neutron per channel per angle, taking account of detector efficiencies and background subtraction. Owing to the spectrometer resolution, the three transitions at $|470|$, $|516|$, and $|537|$ μeV were measured simultaneously as the scattering function was integrated over $|500 \pm 60|$ μeV for each map. For each run the spectra were analyzed with a resolution of ≈ 0.2 Å^{-1}. The maps were symmetrized and extrapolated to a regular grid (81×81). Each pixel covers a substantial part of the Brillouin zone. It is thus impossible to measure the $Q_\parallel$ dependence of the scattering function.

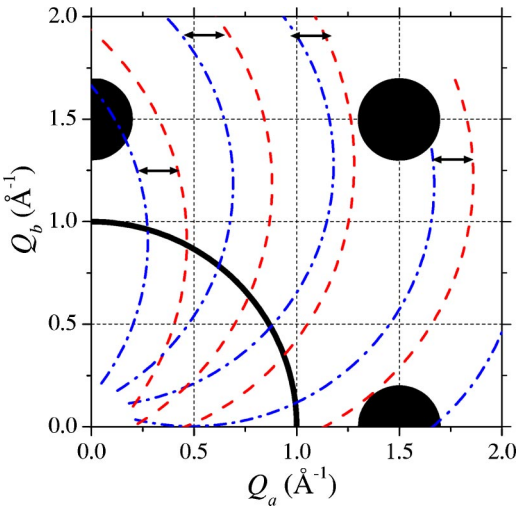

FIG. 6. (Color online) Schematic representation of inelastic scans in the (Q_a, Q_b) plane for various crystal orientations. Dash dot (blue): momentum-transfer trajectories for neutron-energy loss. Dash (red): momentum-transfer trajectories for neutron-energy gain. Arrows point to trajectories for the same crystal orientation. The solid spots with arbitrary diameters correspond to the breather mode transitions for momentum transfer along *a*, or *b*, or for simultaneous transfer along the two directions. The circular ridge of intensity at $|\mathbf{Q}| \approx 1$ Å^{-1} corresponds to tunneling transitions for almost free isotropic rotors.

V. INS SPECTRA: RESULTS

A. Neutron-energy loss (Stokes)

The intensity of excitations arising from the ground state is a maximum for momentum transfer along *a* and *b* (Fig. 7). The pronounced anisotropy is a clear evidence that rotational dynamics are one-dimensional in nature, in total accordance with the crystal symmetry (see above Sec. II). A cut along Q_a (or Q_b) can be decomposed into two Gaussian profiles centered at ≈ 1.0 and 1.55 Å^{-1} with an accuracy of ± 0.2 Å^{-1} (Fig. 8). The full widths at half maximum of each component (0.74 Å^{-1}) were constrained to be identical during the refinement procedure. As these widths are smaller than that of the elastic peak, the contribution of multiple elastic-inelastic scattering events is negligible.

The main component at ≈ 1.55 Å^{-1} in Fig. 8 is very close to that predicted for the $|0\rangle \rightarrow |1\rangle$ transition of breathers (≈ 1.57 Å^{-1}, see above Sec. III B). The observed bandwidth of 0.74 Å^{-1}, which largely exceeds the resolution in Q, is representative of fluctuations of the chain parameter, as $\Delta p_B/p_B = \Delta L/L$. Neglecting the resolution function, we estimate $\Delta L \approx 1.9$ Å. This value is much larger than the square

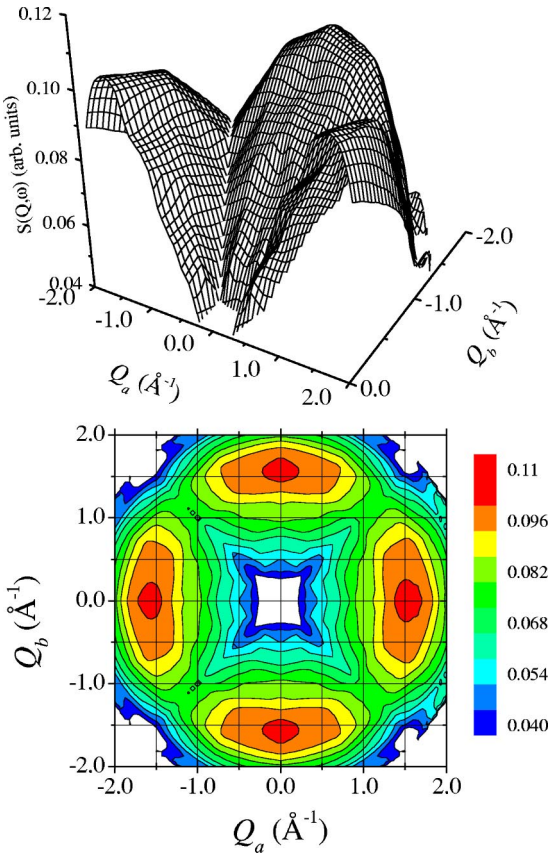

FIG. 7. Landscape view (top) and isointensity contour map (bottom, color online) of $S(Q_a,Q_b,\omega)$ measured in the (a,b) plane of a single crystal of 4-methylpyridine at 1.7 K. Neutron-energy loss $(500\pm60)\,\mu$eV.

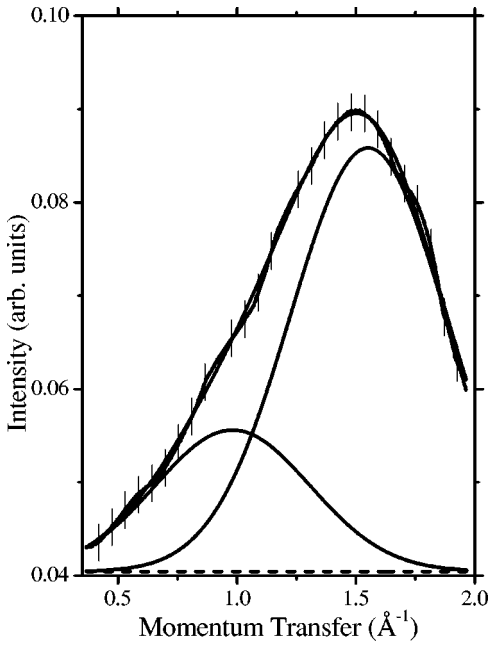

FIG. 8. Profile measured along Q_a (or Q_b) at $(500\pm60)\,\mu$eV (solid line with error bars). Decomposition into two Gaussian profiles (with identical full widths at half maximum of 0.74 Å^{-1}) centered at 0.99 and 1.55 Å^{-1}, respectively, and a constant base line (dash line). The relative areas are 27% and 73% of the total intensity. The calculated profile (solid line) compares to experimental within error bars.

root of the thermal factors for rotational centers of H atoms (see Table V). ΔL is representative of the much greater fluctuations of H$\cdots$H distances between nearest neighbors along the chains arising from zero-point rotational motions. It compares favorably to four times the square root of the zero-point mean-square angular amplitude of methyl groups in the on-site potential: $4\sqrt{\langle r^2\theta^2\rangle}\approx1.8$ Å for rotons at 3.4 meV.[9] On the other hand, the kinetic energy does not depend on L, see Eq. (7). Therefore, the excited breather state in direct space must be regarded as a superposition of dispersionless wave packets localized at each site and whose group velocity is zero. The Fourier transform of the profile in Q gives a Gaussian profile in direct space with full width at half maximum of ≈2.65 Å. This width is much smaller than the full width of the breather wave form of $\approx5\times L\approx20$ Å and even much smaller than the averaged lattice parameter.

The weaker component at ≈1.0 Å^{-1} in Fig. 8 should correspond to the transitions at 470 and 537 μeV, previously attributed to the maxima of the density-of-tunneling states. Compared to the breather band at 1.55 Å^{-1}, this assignment scheme is corroborated by the intensity ratio of $\approx1{:}3$, quite similar to that measured in the energy spectrum.[12] As there is no evidence for any ring of intensity at $|\mathbf{Q}|\approx1$ Å^{-1}, the model based on extended tunneling states in an energy-band structure, Eq. (2), is not confirmed. On the other hand, the similarity of the bandwidths suggests that these transitions also arise from pseudoparticles traveling along the chains (see below Sec. VI).

B. Neutron-energy gain (anti-Stokes)

The scattering function for transitions arising from excited states with long lifetimes compared to the duration of the experiments is also markedly anisotropic (Fig. 9). However, the ridges of intensity are oriented at $\pm45°$ with respect to the *a* or *b* crystal axis, while valleys of intensity are observed for momentum transfer along *a* or *b*. The maps in Figs. 9 and 7 are remarkably complementary. As the **Q** trajectories for each crystal orientation are similar for energy gain and energy loss (see Fig. 6), this complementarity is significant. Therefore, excited traveling states along *a* or *b* are unstable and vanish rapidly.

The ridges of intensity oriented at $\pm45°$ can be assigned to long-lived ''twin excitations'' composed of two elementary excitations traveling coherently along *a* and *b*, respectively. For ''twin breathers'' the maximum of intensity should occur at $|\mathbf{Q}|\approx2.25$ Å^{-1} (see Fig. 6), but this is beyond the measured **Q** range. Another peak at $\approx|1.4|$ Å^{-1} arising from coherent excitations at $\approx|1|$ Å^{-1} along *a* and *b* is quite possible. Unfortunately, the *Q* range is too limited, compared to the peak positions, to propose a profile analysis analogous to that presented in Fig. 8.

VI. MULTISOLITONS

Both anisotropy of the scattering function and vanishing intensity of ''tunneling'' transitions[11] oppose the existence of

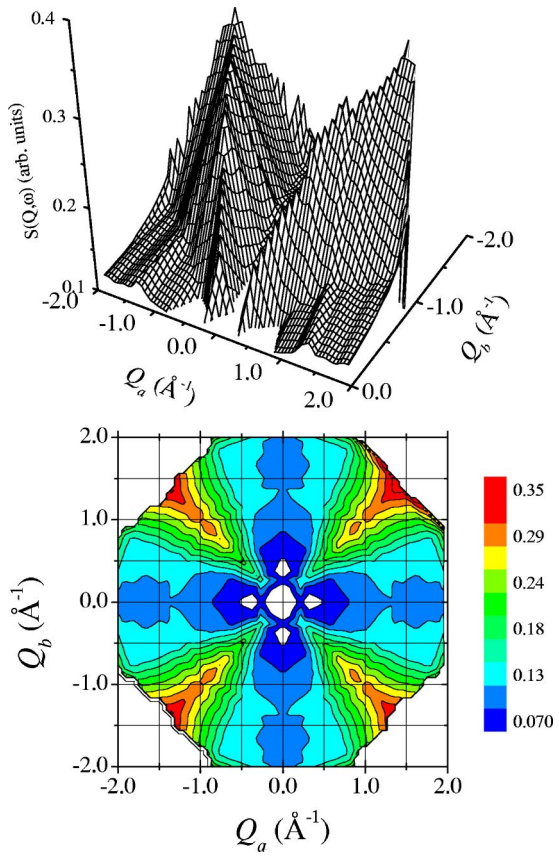

FIG. 9. Landscape view (top) and isointensity contour map (bottom, color online) of $S(Q_a,Q_b,\omega)$ measured in the (a,b) plane of a single crystal of 4-methylpyridine at 1.7 K. Neutron-energy gain (500 ± 60) μeV.

Bloch's states. With hindsight we now understand that proton permutation via tunneling arising from topological degeneracy cannot be represented with small amplitude displacements in the potential expanded to second-order around the equilibrium position because the cyclic boundary condition does not hold. As opposed to that, collective tunneling can be characterized with a topological index $\mathcal{I}$ related to the number of permutations along the chain.

Within the framework of the quantum sine-Gordon theory, extended to Eq. (1), collective tunneling can be represented with long-lived metastable pseudoparticles, composed of kinks or antikinks, traveling along the chain. As the energy for the creation of a pair (a kink and an antikink at rest) from a breather is $\approx$5.32 meV ($\approx$65 K),[9] only pseudoparticles created at high temperature can be observed, provided they survive for sufficiently long time at a low temperature. The decreasing population, as time is passing, of these metastable pseudoparticles should be parallel to the decaying intensities. However, very little is known about the interplay of kinks, antikinks, and rotational tunneling in the quantum regime and we propose a model in Sec. VI A. In order to avoid tedious repetitions in the remainder of this paper, "ksoliton" is used to designate indifferently kinks or antikinks, whenever it is needless to distinguish these excitations. On the one hand, ksolitons are dimensionless and stationary states should give a discrete energy spectrum analogous to Eq. (7) for the breather. On the other hand, as the translation of ksolitons is equivalent to rotation of methyl groups, these pseudoparticles should obey an additional conservation rule related to the angular momentum.

A. Collective tunneling

Stationary states for ksolitons occur if $\lambda_K=L/n_K$. Furthermore, barring states at higher energy corresponding to collective rotation, we suppose that only states within the tunneling energy band are stationary. Then, the energy spectrum can be written as

$$E_{op}\leqslant E_K(n_K)=\sqrt{E_{0K}^2+n_K^2\hbar^2\omega_c^2}\leqslant E_{op};$$

$$n_K=0,\pm1,\pm2,\ldots\ . \tag{8}$$

However, as the first stationary state at $\approx$719 μeV is quite beyond the allowed energy band, single ksolitons cannot account for the observed tunneling bands.

In order to increase the energy at rest, and thus decrease the kinetic energy, we call the integrability of the sine-Gordon equation to introduce pseudoparticles composed of an integer number "N" of ksolitons moving at the same velocity. These "N-ksolitons" are themselves solitons,[26–28] and we suppose that they are also solitonlike solutions of the fully periodical Hamiltonian (1), at least to a level of accuracy compatible with experimental observations in the 4MP crystal. In the absence of many-particle effects, the energy at rest of an N-ksoliton is NE_{0K}, the wavelength associated with this pseudoparticle is $\lambda_{NK}=L/n_{NK}$, and the energy spectrum is

$$E_{op}\leqslant E(N,n_{NK})=\sqrt{N^2E_{0K}^2+n_{NK}^2\hbar^2\omega_c^2}\leqslant E_{ip};$$

$$n_{NK}=0,\pm1,\pm2,\ldots\ . \tag{9}$$

If the kinetic energy is very small compared to the energy at rest, then

$$E(N,n_K)\approx NE_{0K}+\mathcal{E}_{K0}-\frac{\mathcal{E}_{K0}^2}{2NE_{0K}}\cdots, \tag{10}$$

with $\mathcal{E}_{K0}=n_{NK}^2\hbar^2\omega_c^2/2NE_{0K}\approx0.742n_{NK}^2/N$ in meV units. The second- and higher-order terms are relativistic corrections to the classical kinetic energy $\mathcal{E}_{K0}$. The correction for a single ksoliton is -13 μeV. It decreases rapidly with increasing N values.

In addition, translational dynamics of N-ksolitons are related to the symmetry of the tunneling states $|0_{E\pm}\rangle$. These states have opposite angular momenta and, as a consequence of proton indistinguishability, only states whose total angular momentum is zero are allowed. Therefore, except for pseudoparticles composed of equal numbers of kinks and antikinks ($\mathcal{I}=0$), only states with $k_\parallel=0$ are allowed.[33] They may correspond either to two identical pseudoparticles with opposite $k_\parallel$ values or to multiquantum states of single pseudoparticles (see Table VI).

TABLE VI. Comparison of traveling states of *N*-solitons with observed frequencies.

n_{NK}												
1			2			3			4			
N	NE_K (meV)	Calc (μeV)	N	NE_K (meV)	Calc (μeV)	N	NE_K (meV)	Calc (μeV)	N	NE_K (meV)	Calc (μeV)	Obs (μeV)
			11 [a]	126.5	539				22	253.0	539	539 (Ref. 12)
									23	264.5	515	514 (Ref. 11)
3 [a]	34.5	493	6	69.0	493				24	276.0	494	≈500 (Ref. 29)
			12[a]	138.0	494	14 [b]	161	476	25	287.5	474	472 (Ref. 12)

[a]Two pseudoparticles with opposite $k_\parallel$ values.
[b]Only for $\mathcal{I}=0$ and $k_\parallel=2\pi/L$.

For $n_{NK}=1$, there is no stationary state within the allowed energy band for single pseudoparticles. There is a stationary state calculated at ≈ 0.493 μeV for two identical pseudoparticles with $N=3$.

For $n_{NK}=2$, there is only one stationary state at 493 μeV for single particles with $N=6$. All of the 2^6 combinations of kinks and antikinks are suitable for the two-quantum state at $k_\parallel=0$. Besides, eight pseudoparticles composed of three kinks and three antikinks comply with the conservation of angular momentum ($\mathcal{I}=0$) and can occupy the single-particle state at $k_\parallel=\pm 2\pi n_{NK}/L \approx 3.1$ Å^{-1} and $k_\perp=1/r$. As this is far beyond the accessible range, these states are irrelevant. States for two pseudoparticles occur for $N=11$ (539 μeV) and $N=12$ (494 μeV).

For $n_{NK}=3$, stationary states are forbidden for single particles with $\mathcal{I}\neq 0$. Single particles with $N=14$ and $\mathcal{I}=0$ may appear at 476 μeV. The kinetic momentum is either $k_\parallel=2\pi/L$, identical to the breather, or $6\pi/L$, far beyond the accessible range. Multiparticle states are forbidden.

For $n_{NK}=4$, there are four possible N values for single particles (see Table VI). The bands observed at 539 and 472 μeV correspond rather well to $N=22$ and 25, respectively. Frequencies calculated for $N=23$ and $N=24$ are also close to those previously reported.[11,29] The overall agreement, to within a few μeV, is quite satisfactory and confirms that the states at 472 and 539 μeV are quite close to the edges of the energy band. There are seven two-particle states for N ranging from 44 to 50. Four of them coincide with the single-particle states and, therefore, cannot be distinguished. The three additional states (not reported in Table VI for the sake of clarity) calculated at 527, 505, and 484 μeV are not observed. We conclude that these two-particle dynamics have a very low probability.

Finally, for $n_{NK}>4$, the many allowed N values should give rise to a state manifold which is not observed. We conclude that the spectrum is totally dominated by single-particle states for $n_{NK}=4$. The spots of intensity at $Q\approx 1$ Å^{-1} in Fig. 7 can be thus assigned to stationary states of *N*-ksolitons. As there is no constraint for the topological index, these pseudoparticles can be composed of any number of kinks ($N_+ \leqslant N$) and antikinks ($N_- = N - N_+$). The spots observed for momentum transfer along *a* correspond to excitations of chains parallel to *b*, and conversely. The bandwidth in *Q*, similar to that for the breather, is due to the zero-point fluctuation of *L*. According to Eq. (9), there is no dispersion in energy and this is in accordance with spectra obtained at high resolution: the observed bandwidths of ≈ 1 μeV is primarily due to the instrument resolution.[11] In direct space, *N*-ksolitons, in the same way as breathers, are superposition of nondispersive wave packets with full width at half height ≈ 2.65 Å located at the chain sites.

B. Bound states

Bound states account for the existence of excitations traveling coherently along orthogonal directions (see Fig. 9). These dynamics are unforeseen since there is no stable soliton in two dimensions in the classical sine-Gordon theory.[6,7] In the quantum regime, however, pseudoparticles are not localized, neither on a particular site nor on a particular chain, as they were in the classical world. Plane waves associated with pseudoparticles traveling along chains parallel to *a*, or *b*, are delocalized in the (b, c), or (a, c), plane and may combine into waves corresponding to pseudoparticles with equal kinetic momenta along the two directions. For such twin *N*-ksolitons the energy at rest is $2NE_{0K}$ and the kinetic momentum is $p_{2NK}=\sqrt{2}n_{NK}h/L$. Then, traveling states analogous to Eq. (9) are

$$E_{op} \leqslant E_{2K}(N,n_{NK}) = \sqrt{4N^2E_{0K}^2 + 2n_{NK}^2\hbar^2\omega_c^2} \leqslant E_{ip}, \tag{11}$$

or

$$E_{2K}(N,n_{NK}) \approx 2NE_{0K} + \mathcal{E}_{K0} - \frac{\mathcal{E}_{K0}^2}{4NE_{0K}}\cdots. \tag{12}$$

Energy levels for two correlated single particles are very close to those for one single-particle states, to within the minor relativistic correction. The binding energy of twin particles estimated from Eqs. (10) and (12) is

$$\Delta E(N,n_K) = 2E(N,n_K) - E_{2K}(N,n_K) \approx \mathcal{E}_{K0} - \frac{3\mathcal{E}_{K0}^2}{4NE_{0K}}\cdots. \tag{13}$$

Along the same line of reasoning, the energy spectrum of bound breather states is

$$E_{2B}(n_B)=\sqrt{4E_{0B}^2+2n_B^2\hbar^2\omega_c^2}, \quad \text{with} \quad n_B=0,\pm1,\pm2\ \ldots \tag{14}$$

or

$$E_{2B}(n_B)\approx 2E_{0B}+\mathcal{E}_{B0}-\frac{\mathcal{E}_{B0}^2}{4E_{0B}}\cdots, \tag{15}$$

with $\mathcal{E}_{B0}=n_B^2\hbar^2\omega_c^2/2E_{0B}\approx n_B^2 525\ \mu$eV. The binding energy is close to $\mathcal{E}_{B0}$. Then, the $|1\rangle\rightarrow|0\rangle$ transition calculated at 521 μeV is slightly different from that of a single breather at 517 μeV. However, the relativistic correction of $\approx 4\ \mu$eV is within experimental accuracy. The maximum of intensity at $|\mathbf{Q}|=2\pi\sqrt{2}/L\approx 2.2$ Å^{-1} is on the edge of the measured range, but, owing to the bandwidth, this transition contributes to the ridges of intensity in Fig. 9.

The scenario suggested by Figs. 7 and 9 is that excitations along *a* and *b* created at high temperature merge naturally into bound states, as the crystal is cooled down rapidly. The activation energy for dissociation of bound pseudoparticles ($\approx$0.5 meV or 6 K, in all cases) accounts, at least partially, for the very slow relaxation rate of these states. A pseudoparticle in the bound state with kinetic momentum $[p_a,p_b]$ can split into an unbound state $[p_a,0]$ or $[0,p_b]$ upon quasielastic scattering. This mechanism does not contribute to the measured scattering function. As there is no binding energy for pseudoparticles at rest, bound states are not observed for neutron-energy loss measurements.

VII. DISCUSSION

Collective rotational tunneling for infinite chains is a thermally activated process which disappears at low temperature. The topological degeneracy that gives rise to tunnel splitting of isolated rotors or coupled pairs[23] is canceled in the ground state. Then, the periodicity of the coupling potential in Eq. (1) can be ignored and the sine-Gordon equation is exact. The chain dynamics are represented with a collective angular coordinate and a nonfactorable wave function corresponding to the quantum breather. These dynamics are possible because the uncorrelated pairs of face-to-face methyl rotors in the crystal can be regarded as composed bosons. Otherwise, hydrogenated methyl groups with total nuclear spin $S=\frac{3}{2}$ should obey the Fermi statistic law. Clearly, the pairing of methyl groups and the absence of dynamical coupling within these pairs are key ingredients for the quantum sine-Gordon dynamics in 4MP.

The thermal energy for the creation of a significant density of *N*-ksolitons, with internal energy greater than 250 meV (3000 K), is far beyond the melting point of the 4MP crystal. As a matter of fact, the maximum population density should be less than $\approx 10^{-5}$ per site. This should be undetectable with INS. However, Raman spectra show that collective rotational dynamics appear only below $\approx$100 K,[16] which compares to thermal energy for creation of kink-antikink pairs. Above 100 K, methyl groups are totally uncoupled and rotation is free. As the sample is cooled down, the orientational disorder is quenched in the displacive regime and gives rise to a high density of ksolitons corresponding to staggered methyl groups with respect to on-site equilibrium. Even though only a few of these pseudoparticles are observable with spectroscopy techniques, the significant amount of energy stored in *N*-ksolitons should be relevant for further analysis of thermal properties.

At a low temperature, the decay of *N*-ksolitons is not counterbalanced by any creation process *ex vacuo*. The lifetime of several days for the bands at 539, 514, and 472 μeV[11] is almost infinity on the time scale of rotational tunneling ($\sim 10^{-11}$ s). Even though the band at $\approx$500 μeV (Table VI) was observed only under fast cooling conditions,[29] the lifetime of the order of 1 h is still more than 14 orders of magnitude greater than the tunneling period, and can be regarded as infinity. Indeed, there is no relaxation channel for solitons in the sine-Gordon equation (5) and this is also probably the case for the conservative Hamiltonian, Eq. (1). Moreover, the localization in momentum and energy make quite unlikely dynamical coupling with phonons.

N-ksolitons are heavy pseudoparticles whose masses at rest are in the range of $\approx 150-170$ amu. The relevant internal energies in Table VI are virtually identical to that of the ''Davydov soliton'' supposedly created by excitation of C═O bonds at $\approx$200 meV in polypeptides.[4,5] Similar internal energies have been estimated for nonlinear excitations in polyethylene.[30,31] To the best of our knowledge, these dynamics were treated within the framework of classical mechanics in theoretical works. A critical review on this subject is beyond the scope of the present work. However, from the experimentalist viewpoint, we emphasize that a thorough examination of the scattering function in momentum space is necessary to firmly establish the otherwise rather speculative solitonlike dynamics, because an important consequence of nonlinearity in the quantum regime is localization in reciprocal space. This is a key information for understanding infrared and Raman intensities. Furthermore, the pronounced quantum effects observed for *N*-ksolitons show that these effects should not be ignored without caution. If solitons in polymers are quantum in nature, they should behave as plane waves and stationary traveling states should arise from discreteness. Wave packets in direct space arising from fluctuations of the lattice parameters should not be confused with localization. In any case, the group velocity is zero and there is no propagation, to the least in the absence of a driving force.

The coupling between dipolar magnetization and molecular rotation was observed in 4MP with NMR by Haupt.[32] The effect occurs only below $\approx$45 K. A sudden increase in temperature is followed by the rapid growth and subsequent slow decay of an enormous dipolar signal, about 100 times larger than the equilibrium Zeeman signal. The effect was explained by the coupling of the combined nuclear spin and methyl rotor with the crystal phonons. However, INS experiments show that there is virtually no such coupling. We suggest that *N*-ksolitons offer an alternative explanation. The magnetic momentum due to residual charges on the methyl protons is directly related to the angular momentum. In the absence of an external magnetic field, the degeneracy yields strict cancellation of magnetic momentums. A magnetic field applied along the *c* crystal axis breaks down the degeneracy

and dipolar magnetization arises. The temperature jump increases the population density of *N*-ksolitons and thus accelerates the growth of magnetization. At a low temperature, the polarization should decay as the population of *N*-ksolitons decreases. A magnetic field parallel to the (a,b) plane should have no effect. Therefore, the already spectacular effect previously observed for a powdered sample should be further enhanced for a single crystal. This could be a macroscopic manifestation of *N*-ksolitons in 4MP.

Theoretical studies of generalized Klein-Gordon equations with periodic coupling suggest that rotating modes, another type of nonlinear localized excitation, could occur for an infinite chain of coupled rotors represented with the classical analog to Eq. (1).[18] In contrast to breathers, these modes are highly localized within a few methyl groups rotating rapidly, at energy greater than the effective potential barrier, while the remainder of the chain performs small amplitude oscillations around the local equilibrium position. These excitations are stationary without the possibility of translational motion along the chain. They could be generated by spontaneous localization of thermal energy. As threshold energies for the creation of rotating modes and kinks are similar, these excitations could coexist at thermal equilibrium and one may ask whether rotating modes can be probed with INS. However, to the best of our knowledge, there is no theory for quantum analogs to rotating modes and it is unlikely that such highly localized modes be eigenstates of a periodic lattice. Nevertheless, we speculate that the kinetic momentum distribution for such static excitations should be isotropic in the (a,b) plane. Then, INS experiments give no evidence for such excitations. Moreover, the energy for creation/annihilation of rotating modes is far beyond the tunneling range and the maximum of intensity for rotational levels with large quantum numbers should occur at large $|\mathbf{Q}|$ values, beyond the accessible range. Consequently, tunneling spectroscopy cannot evidence such hypothetical static rotating modes.

VIII. CONCLUSION

The structure of the 4-methylpyridine crystal is compatible with collective rotational dynamics in one dimension. There is no ordering of the face-to-face methyl groups at low temperature, down to 10 K, and correlated rotation of the pairs is forbidden by symmetry. These pairs behave as composed bosons.

In the energy range of rotational tunneling, the inelastic neutron scattering function of a single crystal at 1.5 K is distinctive of rotational dynamics in one dimension. For neutron-energy loss, spots of intensity at Q_a or $Q_b \approx 1.55$ Å^{-1} correspond to stationary traveling states of the quantum sine-Gordon breather. The bandwidth in Q is related to zero-point fluctuations of the chain parameter. In direct space, the dimensionless pseudoparticle is a superposition of dispersionless wave packets at the chain sites with FWHH ≈ 2.65 Å. The group velocity is zero and, therefore, the hope that nonlinearity could give rise to energy localization and transport is not realized in the context of quantum methyl rotation.

For collective tunneling, Bloch's states are forbidden by the topological degeneracy. Pseudoparticles composed of rather large numbers (from 22 to 25) of kinks or antikinks account for collective tunneling. Quantization of the kinetic momentum arises from the periodicity of the chain lattice and stationary states are allowed exclusively within the tunneling energy band. Conservation of the angular momentum gives rise to singularities in momentum space at $k_{\|}=0$ and $k_{\perp}=\pm n_r/r$. In direct space the pseudoparticles are superposition of dispersionless wave packets at the chain sites, analogous to the breather.

N-ksolitons created at high-temperature decay at low temperature. Collective rotational tunneling is a thermally activated process. In the ground state, the topological degeneracy of individual methyl groups is canceled and rotational dynamics are represented with a single collective coordinate throughout the chain.

The plane waves associated with *N*-ksolitons or breathers traveling simultaneously along *a* and *b* directions form bound states. The binding energy may account for the virtually infinite lifetime of these excited states. In the ground state, there is no binding energy for pseudoparticles at rest.

These experiments emphasize the distinctive properties of nonlinear excitations in one dimension, in the quantum regime. The chain discreteness gives rise to discrete spectra in both energy and momentum. Dimensionless nondispersive pseudoparticles are fully delocalized waves. Broadening of the wave packet in momentum is correlated to zero-point fluctuations of the chain parameter. In direct space ideal planar waves for a rigid lattice turn into a superposition of nondispersive wave packets whose group velocity is zero.

ACKNOWLEDGMENTS

We thank G. J. Kearley for assistance during INS experiments and data analysis at ILL, and J. Goddard for growing single crystals.

*Electronic address: fillaux@glvt-cnrs.fr

[1] A.J. Sievers and S. Takeno, Phys. Rev. Lett. **61**, 970 (1988).
[2] R.S. MacKay and S. Aubry, Nonlinearity **7**, 1623 (1994).
[3] A. Scott, *Nonlinear Science: Emergence and Dynamics of Coherent Structures* (Oxford University Press, Oxford, 1999).
[4] A.S. Davydov, J. Theor. Biol. **38**, 559 (1973).
[5] P.-A. Lindgård and A.M. Stoneham, J. Phys.: Condens. Matter **15**, V5 (2003).
[6] R. Rajaraman, *Solitons and Instantons. An Introduction to Solitons and Instantons in Quantum Field Theory* (North-Holland, Amsterdam, 1989).
[7] Y.S. Kivshar and B.A. Malomed, Rev. Mod. Phys. **61**, 763 (1989).
[8] R.F. Dashen, B. Hasslacher, and A. Neveu, Phys. Rev. D **11**, 3424 (1975).
[9] F. Fillaux and C.J. Carlile, Phys. Rev. B **42**, 5990 (1990).
[10] F. Fillaux, C.J. Carlile, and G.J. Kearley, Phys. Rev. B **44**, 12 280 (1991).

[11] F. Fillaux, C.J. Carlile, J. Cook, A. Heidemann, G.J. Kearley, S. Ikeda, and A. Inaba, Physica B **213& 214**, 646 (1995).
[12] F. Fillaux, C.J. Carlile, and G.J. Kearley, Phys. Rev. B **58**, 11 416 (1998).
[13] U. Ohms, H. Guth, W. Treutmann, H. Dannohl, A. Schweig, and G. Heger, J. Chem. Phys. **83**, 273 (1985).
[14] C.J. Carlile, B.T.M. Willis, R.M. Ibberson, and F. Fillaux, Z. Kristallogr. **193**, 243 (1990).
[15] E. K. Morris, Ph.D. thesis, Université d'Orsay, 1997.
[16] N. LeCalvé, B. Pasquier, G. Braathen, L. Soulard, and F. Fillaux, J. Phys. C **19**, 6695 (1986).
[17] M. Plazanet, M.A. Neumann, and H.P. Trommsdorff, Chem. Phys. Lett. **320**, 651 (2000).
[18] S. Takeno and M. Peyrard, Physica D **92**, 140 (1996).
[19] See www-llb.cea.fr
[20] D. J. Watkin, C. K. Prout, R. J. Carruthers, P. W. Betteridge, and R. I. Cooper, CRYSTALS version 11. (Chemical Crystallography Laboratory, University of Oxford, Oxford, England, 2002).
[21] V.F. Sears, Neutron News **3**, 26 (1992).
[22] B. Nicolaï, G.J. Kearley, A. Cousson, W. Paulus, F. Fillaux, F. Gentner, L. Schröder, and D. Watkin, Acta Crystallogr., Sect. B: Struct. Sci. **57**, 36 (2001).
[23] B. Nicolaï, A. Cousson, and F. Fillaux, Chem. Phys. **290**, 101 (2003).
[24] A. Péneau, M. Gourdji, and L. Guibé, J. Mol. Struct. **111**, 227 (1983).
[25] See www.ill.fr/YellowBook/IN5/welcome.html
[26] R. Hirota, J. Phys. Soc. Jpn. **33**, 1459 (1972).
[27] P.J. Caudrey, J.D. Gibbon, J.C. Eilbeck, and R.K. Bullough, Phys. Rev. Lett. **30**, 237 (1973).
[28] M.J. Ablowitz, D.J. Kaup, A.C. Newell, and H. Segur, Phys. Rev. Lett. **30**, 1262 (1973).
[29] C.J. Carlile, S. Clough, A.J. Horsewill, and A. Smith, Chem. Phys. **134**, 437 (1989).
[30] A.V. Savin and L.I. Manevitch, Phys. Rev. B **58**, 11 386 (1998).
[31] A.V. Savin and L.I. Manevitch, Phys. Rev. B **67**, 144302 (2003).
[32] J. Haupt, Phys. Lett. **38A**, 389 (1972).
[33] Breather traveling states are also degenerate with respect to the propagation direction but the internal harmonic oscillation has no angular momentum. It is thus possible to distinguish traveling states by transferring momentum along a particular direction. In this context, the breather is more closely related to phonons than to collective tunneling.